FINAL TECHNICAL REPORT

GRANT NAG 5-18

UPPER MANTLE HETEROGENEITY: COMPARISONS OF REGIONS SOUTH OF AUSTRALIA WITH PHILIPPINE BASIN

The goal of this study has been to attempt to identify the nature of mass anomalies that may occur beneath the regions of negative residual depth anomalies in the region south of Australia and in the Philippine Basin. These two locations were selected because one of them (south of Australia) has an anomalously fast surface wave velocity structure, and the other (Philippine Basin) has an anomalously slow surface wave velocity structure.

Available seismic refraction data south of Australia indicates that the crust is not exceptionally thin, but has near normal oceanic thicknesses. Available data for the West Philippine Basin indicates that the crust is about 1 km thinner than Pacific Ocean crust of the same age, but is not sufficiently thin to isostatically account for the 1 km residual depth anomaly. Thus the causes of the negative residual depths presumably lie in the upper mantle. Assuming the hypothesis that most upper mantle density anomalies are thermal in nature would suggest colder than normal mantle beneath regions having negative depth anomalies. If this is so, then a positive gravitational attraction due to the excess density of the cold mantle would be expected, and might provide the compensation for the mass deficiency owing to the excess water depth. Because the topographic mass anomaly is closer than the upper mantle mass anomaly, observed free-air anomalies would be slightly negative even for perfect isostasy. Numerical

model studies of convection in the upper mantle also predict a positive correlation between residual elevation and free-air gravity anomalies. No obvious correlation with long wavelength free-air gravity anomalies has been observed south of Australia, and a region of slightly negative anomalies occurs in the West Philippine Basin.

Under other funding, we have recently identified that for each spherical harmonic degree, the ratio of the gravity contribution to the geoid contribution is a greater constraint on dimensions and depth of possible source masses than is the wavelength associated with the zonal harmonics. This realization has led to a plausible decomposition of the earth's gravity field (Bowin, 1980, in prep.). This decomposition suggests that the mass anomalies due to topography at the core-mantle boundary are predominantly contained in the coefficients for the second and third harmonics, and that the harmonics 4 through 10 contain information on mass anomalies in the mantle -- largely below 300km depth. The combined contributions from degree 4 through 10 yield a narrow belt of positive geoid anomalies coincident with most of the world's sites of plate convergence. That positive anomaly may result from mass excesses associated with subducted cold lithosphere. By subtracting a degree 10 field from radar altimeter geoid observations, the contributions from mass anomalies at the core-mantle boundary, and from the deeper parts of subduction zones and of the mantle are largely removed. The residual geoid anomalies are thus restricted to those resulting from mass anomalies in the outer 600km of the earth as would all mass anomalies contributing to degrees 11 and higher on the basis of their gravity to geoid ratio.

To better evaluate the specific regional spherical harmonic field to remove in localized studies we plotted cummulative contribution curves for the Philippine Basin and the region south of Australia (Figure 1 and 2). From the cummulative contribution curves, a spherical harmonic degree 10 field was selected for the Philippine Basin for subtraction of a regional field best representing mass anomalies of the earth and the very broad wavelength anomaly presumed to be due to the subducted lithosphere slab at the Marianna arc/trench system. A spherical harmonic degree 13 field was selected for the region south of Australia. These spherical harmonic representations of a regional field were subtracted from GEOS-3 geoid data. Contoured maps of the resulting residual geoid maps are shown in Figures 3 and 4.

The residual geoid anomaly maps show a positive anomaly associated with the residual depths south of Australia, and a negative anomaly associated with the West Philippine Basin. The residual geoid anomalies are consistent with the anomalous surface wave velocities, and with a thermal origin, but obviously not then with residual depth. The pattern of positive residual geoid anomaly in the region south of Australia, however, differs from the northeast trending negative residual depth anomaly as presented by Cochran and Talwani (1977). The site of the greatest residual depth anomaly (-1,000m) lies beneath the east-west trending residual geoid low immediately south of the Australian shelf. Further examination of the data is required.

The residual geoid low in the Philippine Basin is consistent with the area of negative free-air gravity anomalies seen in the map of Watts et al. (1978) and the area of deep water (depths greater than 5900m) in the West Philippine Basin (Mammerickx, 1976). Comparing the ratio of the regional free-air gravity anomaly to the residual geoid anomaly with that due to

thin horizontal disks suggested a depth to the anomalous mass source of about 200km; that is, considerably below the base of the lithosphere. However, more rigorous modeling, particularly one incorporating an upper mantle mass excess as isostatic compensation for excess water depths was needed. We pursued such an investigation using theoretical admittance functions, and a preprint of the resulting paper is appended to this report. A summary of these results will be given at the end of this report.

Under this grant we have recently succeeded in developing an interpolation scheme utilizing correlation functions that together with our geographic organized data files allow estimation of geoid and gravity values at any selected location. The first results obtained using this technique are shown in Figures 5, 6 and 7: profiles of GEOS-3 geoid, free-air gravity anomalies from surface ship data, and bathymetry along Latitude 20^{o}N were constructed. Computed GEM-9 geoid and gravity fields to degree 10 were then subtracted from the interpolated values to obtain the profiles of residual geoid and gravity along 20^{o}N latitude. We have subsequently learned how to better tune the interpolation parameters and now can obtain better estimates (See Fig. 8 for example of improvement). This interpolation technique also provides error estimates for each value (Fig. 8). This capability is very important for quantitative analysis of the geoid and gravity data.

The ability explained above to retrieve good estimates of geoid and gravity anomalies at preselected locations and thus construct any desired profile or grid will be used to experiment in the combined inversion of residual geoid and gravity data to obtain estimates of the dimensions and depth of the mass anomalies causing the geoid and gravity anomalies.

In summary, residual geoid anomalies in association with negative residual depth anomalies have been identified in the Philippine Basin (negative) and in the region south of Australia (positive and negative). In the latter region the geoid anomalies have eastward trends whereas the depth anomaly trends northeast. The surface wave velocity data should now be re-examined to see how they may fit to this new finding. The residual geoid anomaly is positive in the vicinity of the crest of the southeast Indian ridge where the anomalously fast surface wave velocity data seems best defined, and anomalously cool upper mantle could explain both. However, if this cool mantle were the cause of the excess water depths, negative geoid and gravity anomalies would be expected. In the Philippine Basin, the negative residual geoid anomaly is consistent with a thermal cause for the slow surface wave velocity structure, but if so, then a warm (slow) upper mantle would not be an explanation for the excess water depth (negative residual depth) anomalies in the Philippine Basin.

Theoretical gravity-topography and geoid-topography admittance functions indicate that for the Philippine Sea region high density mantle at about 60 km depth can account for the magnitudes of the gravity and residual geoid anomaly and the 1 km residual water depth anomaly. In that case, however, dense upper mantle material would be contrary to the anomalously slow surface wave velocity structure in the Philippine Sea as determined by Seekins and Teng (1977), although it could be compatible with a normal surface wave velocity structure in the west Philippine Basin as determined by Sacks and Shione (1981). Alternatively, the negative residual depth anomaly may be compensated for by excess density in the uppermost mantle, but the residual geoid and regional free-air gravity anomalies and a slow

surface wave velocity structure might result from low-density warm upper mantle material lying beneath the zone of high-density uppermost mantle. From a horizontal disk approximation, the depth of the low-density warm mantle is estimted to be on the order of 200 km.

Both the negative depth anomaly and the compensating mass excess in the uppermost mantle may have developed in the Eocene as the lithosphere of the west Philippine basin formed. Heating of the deeper upper mantle which could cause slow surface wave velocities and the negative gravity and geoid anomalies may be a much younger phenomenon and presently be in progress.

References Cited

Bowin, C.O., 1980. Why the Earth's greatest geoid anomaly is so negative, (abs.), EOS (Am. Geophys. Union Trans.), v. 61 (17), p. 209.

Cochran, J.R. and M. Talwani, 1977. Free-air gravity anomaly in the world's ocean and their relationship to residual elevation, Geophys. J. Roy. astr. Soc., 50, 495-552.

Mammerickx, J., et al., 1976. Bathymetry of the east and southeast Asian seas: Geol. Soc. America Map Chart Series MC-17, scale 1:6,442,194.

Sacks, I.S. and K. Shiono, 1981. Structure of the Philippine Sea Plate from Surface Waves, EOS, Vol. 62, No. 17, p. 326.

Seekins, L.C. and T. Teng, 1977. Lateral variations in the structure of the Philippine Sea Plate, J. Geophys. Res., 82, 317-324.

Watts, A.B., C. Bowin and J. Bodine, 1978. Free-air gravity field in a Geophysical Atlas of the East and Southeast Asian Seas, The Geological Society of America, Inc., Map and Chart Series MC-25. Scale: 1:6,442,194.

FIGURE CAPTIONS

Figure 1 Cumulative geoid anomaly curves for 15 sites in the Philippine Basin region. Computed from GEM-9 spherical harmonic coefficients. Numbers below lower right curve indicate harmonic degree.

Figure 2 Cumulative geoid anomaly curves for 12 sites in the region south of Australia. Computed from GEM-9 spherical harmonic coefficients. Numbers below lower right curve indicate harmonic degree.

Figure 3 Residual geoid anomalies of the Philippine Basin region. Obtained by removing a GEM-9 spherical harmonic degree 10 field from GEOS-3 observations. Contour interval is 1 meter.

Figure 4 Residual geoid anomalies of region south of Australia. Obtained by removing a GEM-9 spherical harmonic degree 13 field from GEOS-3 observations. Contour interval is 1 meter.

Figure 5 Profiles of geoid anomaly, free-air gravity anomaly, and bathymetry across the Philippine Basin along Latitude 20^{o}N. Data obtained by interpolation using objective analysis techniques.

Figure 6 Profiles regional geoid and gravity profiles computed from GEM-9 spherical harmonic coefficients through degree 10. Same location as for Figure 5.

Figure 7 Profiles of residual geoid anomaly, residual free-air gravity anomaly, and bathymetry, obtained by subtracting regional fields (Fig. 6) from observed data (Fig. 5).

Figure 8 Profile of geoid anomaly across the Philippine Basin along Latitude 20^{o}N. Interpolated values as in Fig. 5 but with 1% noise assumed (top). (Middle) profile is number of GEOS-3 observations used in each interpolation. (Bottom) profile is predicted error in dimensionless values reflection distribution of data observations for each interpolation.

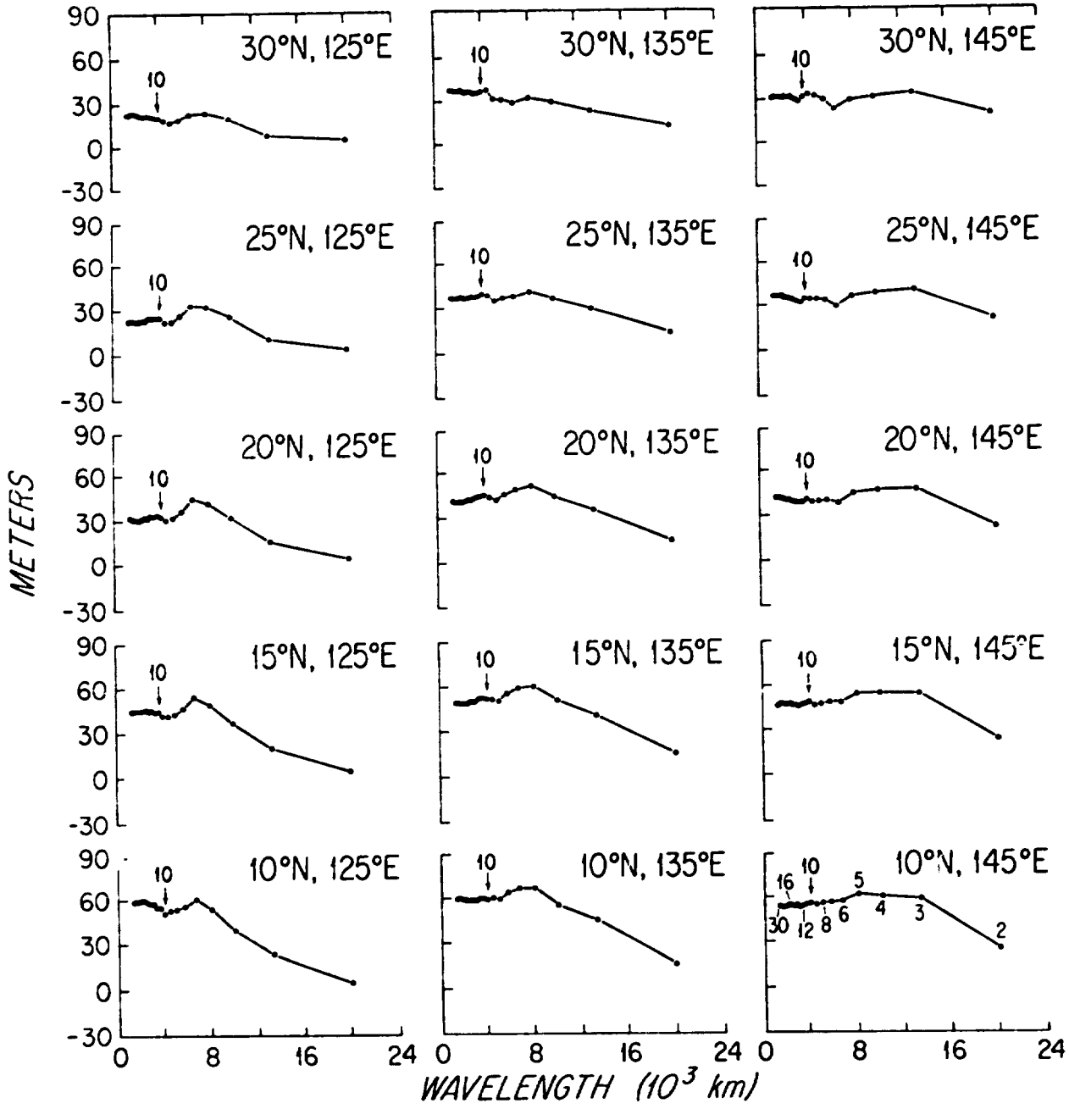
30°N, 125°E
30°N, 135°E
30°N, 145°E
25°N, 125°E
25°N, 135°E
25°N, 145°E
20°N, 125°E
20°N, 135°E
20°N, 145°E
15°N, 125°E
15°N, 135°E
15°N, 145°E
10°N, 125°E
10°N, 135°E
10°N, 145°E
90
60
30
0
-30
10
16
30
12
8
6
5
4
3
2
0
8
16
24
METERS
WAVELENGTH (10³ km)

1 of 1

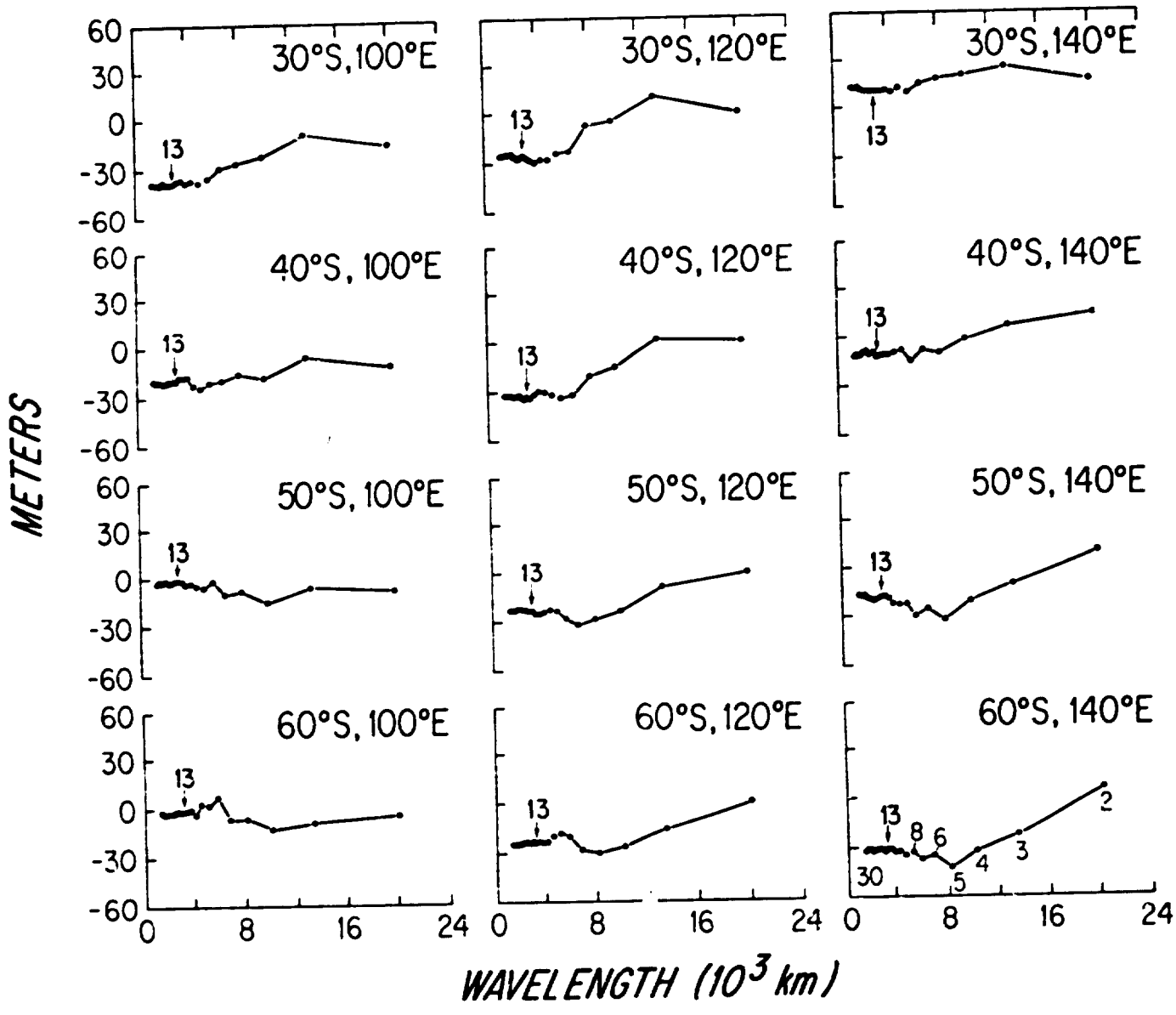
30°S, 100°E
30°S, 120°E
30°S, 140°E
40°S, 100°E
40°S, 120°E
40°S, 140°E
50°S, 100°E
50°S, 120°E
50°S, 140°E
60°S, 100°E
60°S, 120°E
60°S, 140°E
METERS
WAVELENGTH (10³ km)
60
30
0
-30
-60
0
8
16
24
13
8
6
4
3
2
5
30

2 of 4

fig 3

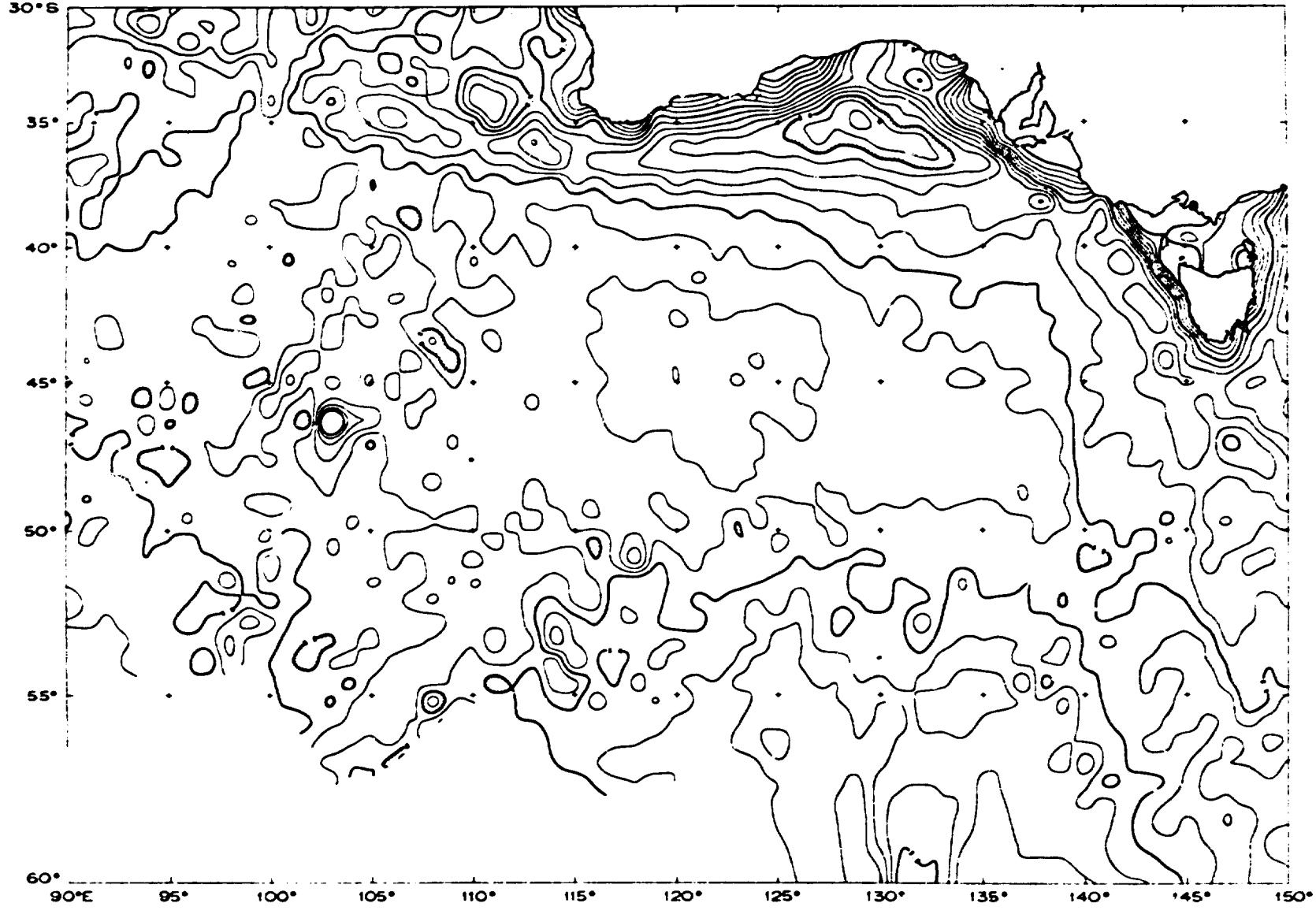
30°S
35°
40°
45°
50°
55°
60°
90°E
95°
100°
105°
110°
115°
120°
125°
130°
135°
140°
145°
150°

Fig 1

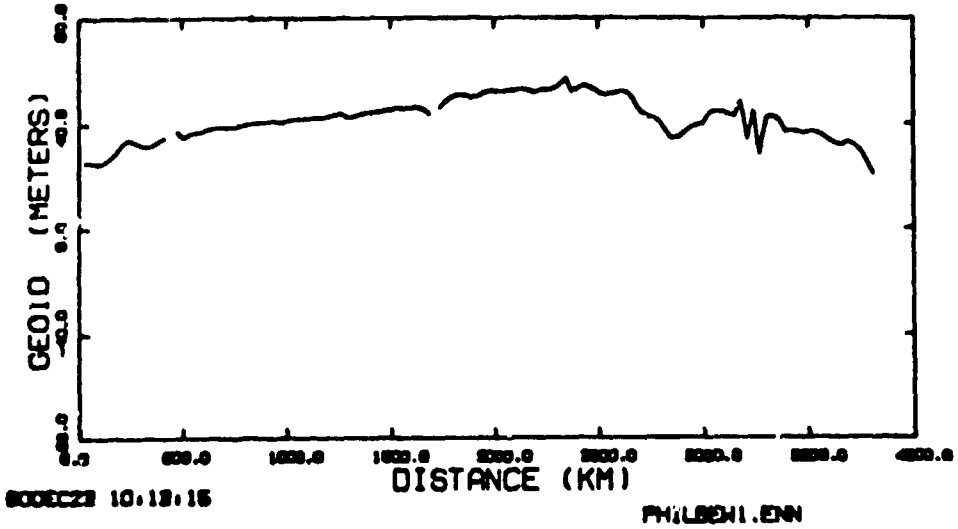
GEOID (METERS)
DISTANCE (KM)

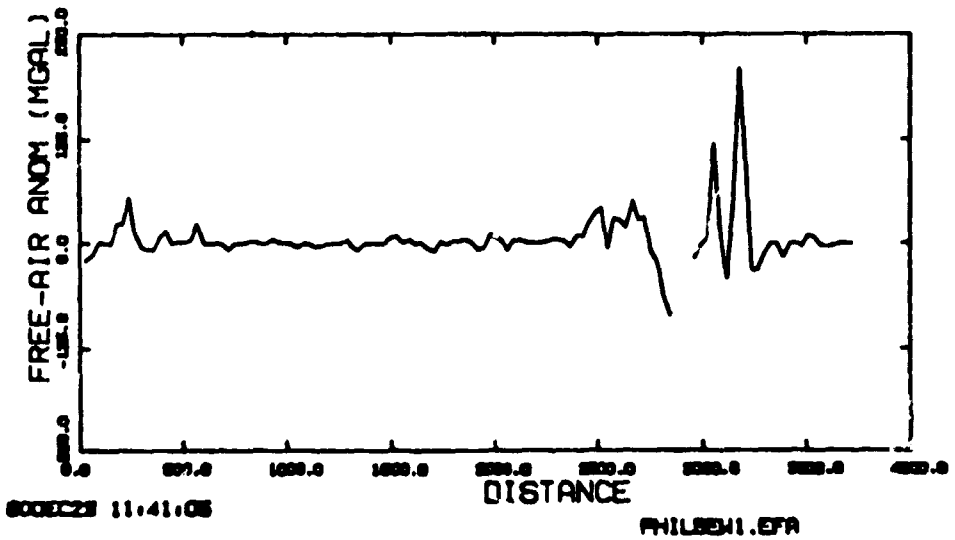
FREE-AIR ANOM (MGAL)
DISTANCE

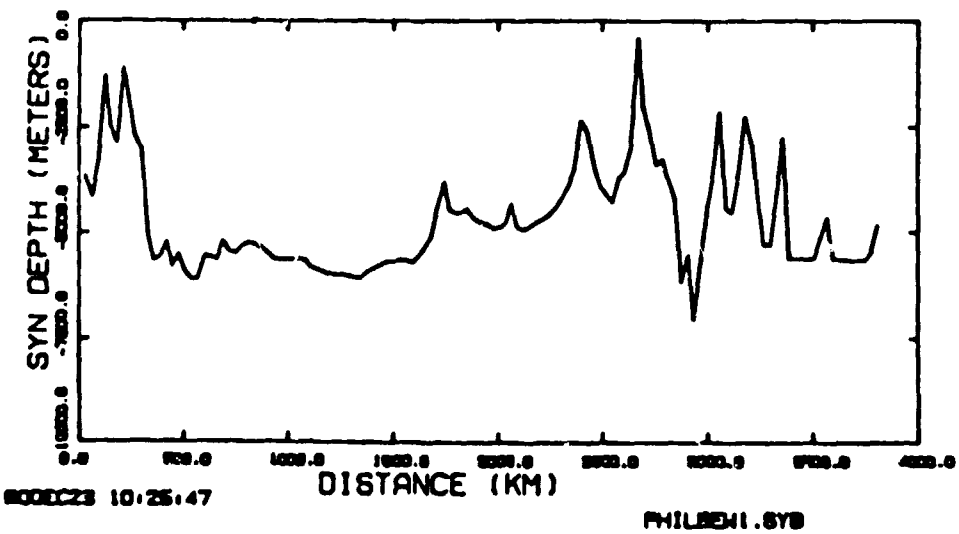
SYN DEPTH (METERS)
DISTANCE (KM)

fig 5

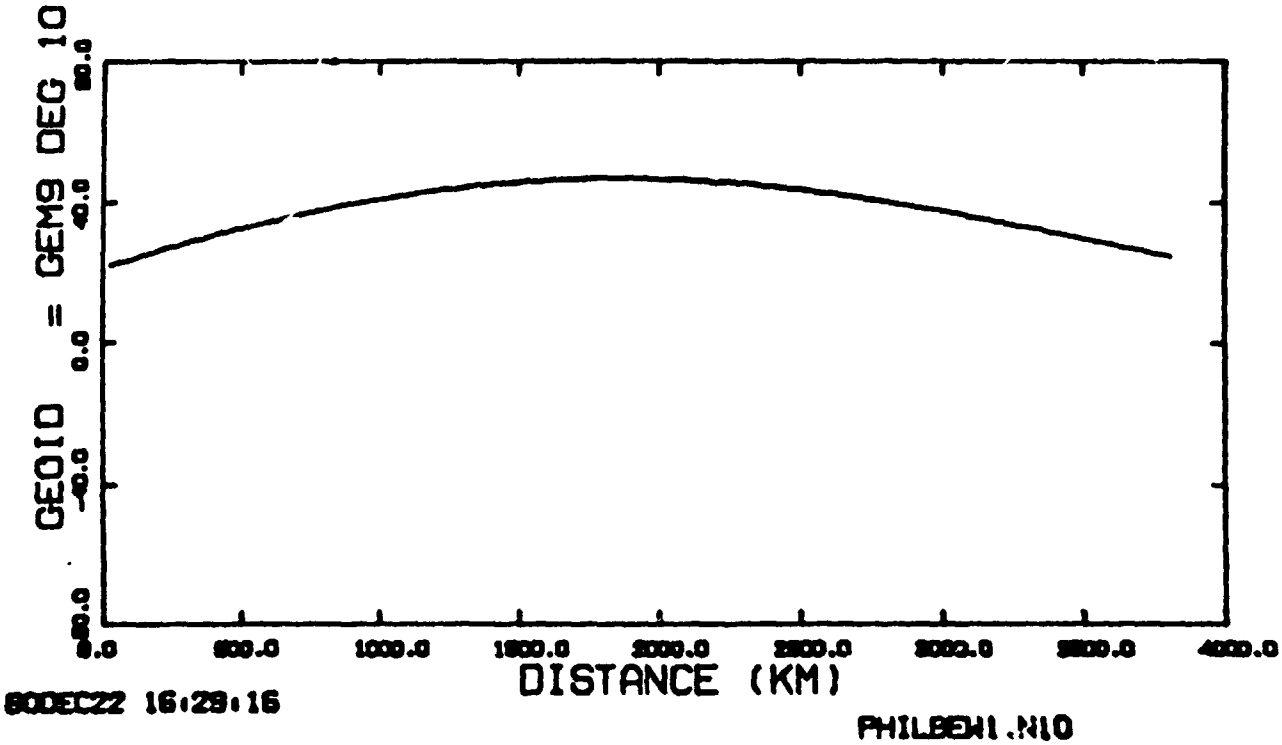

80DEC22 16:29:16

PHILBEH1.N10

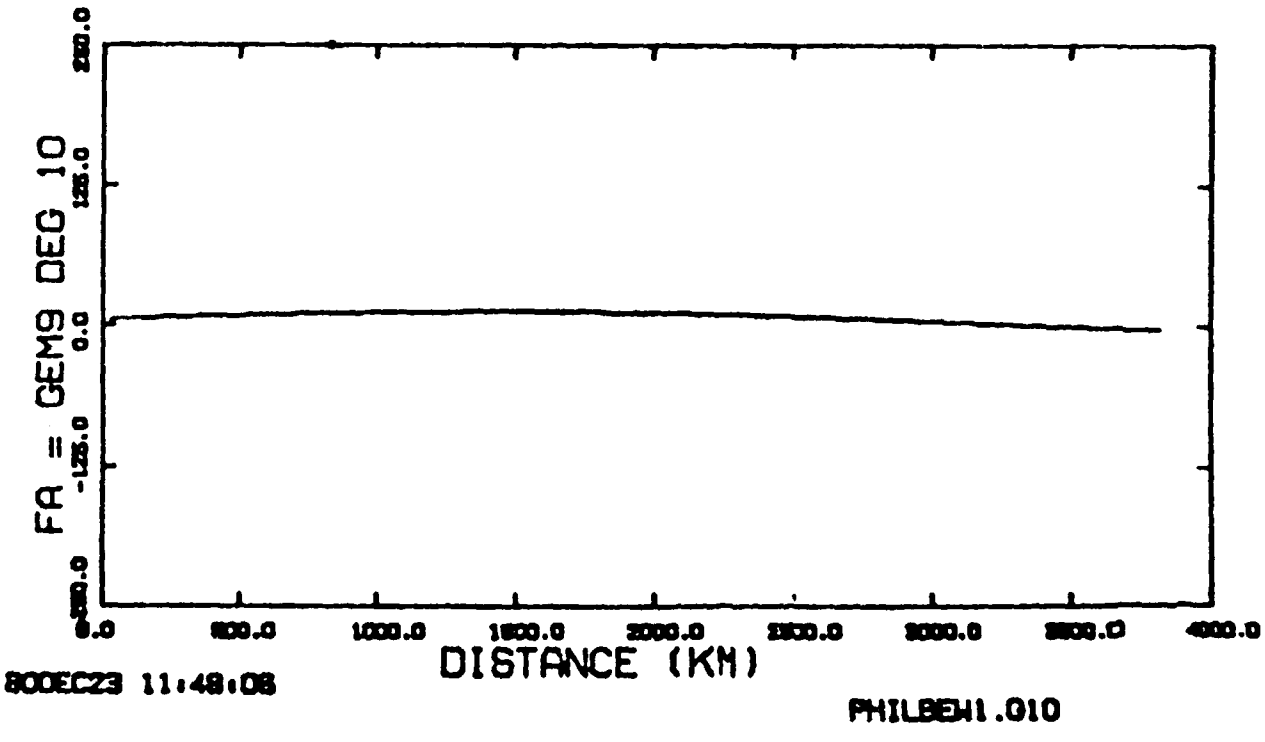

80DEC23 11:48:08

PHILBEH1.G10

fig 6

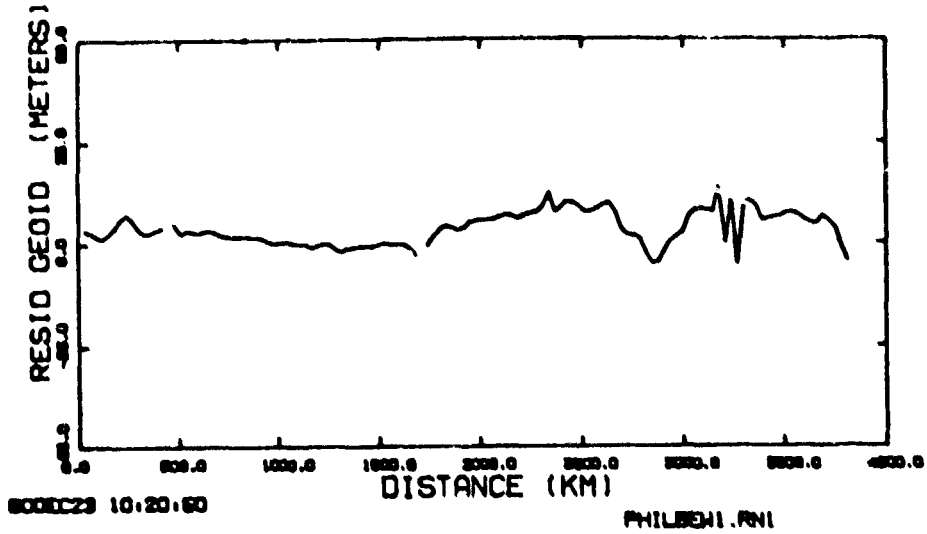
RESID GEOID (METERS)
DISTANCE (KM)
PHILBEH1.RN1

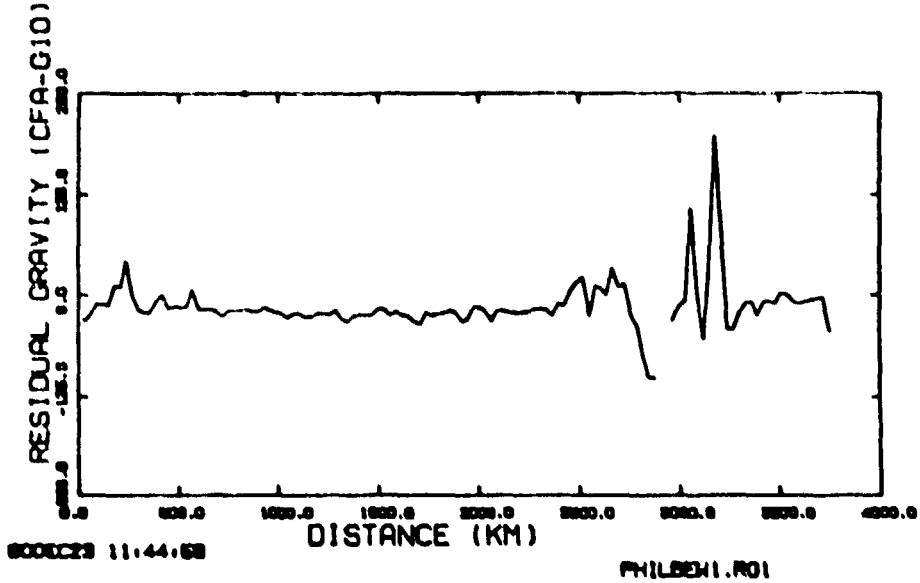
RESIDUAL GRAVITY (CFA-G10)
DISTANCE (KM)
PHILBEH1.R01

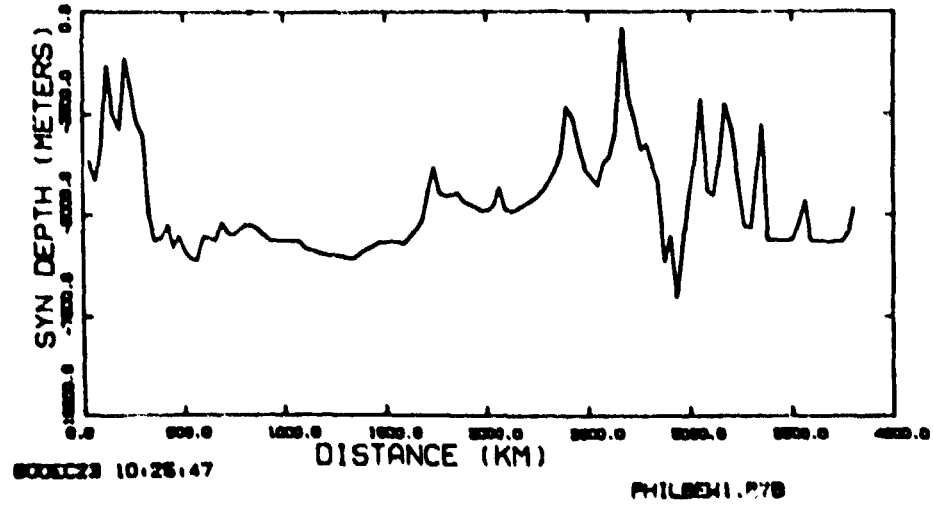
SYN DEPTH (METERS)
DISTANCE (KM)

fig 7

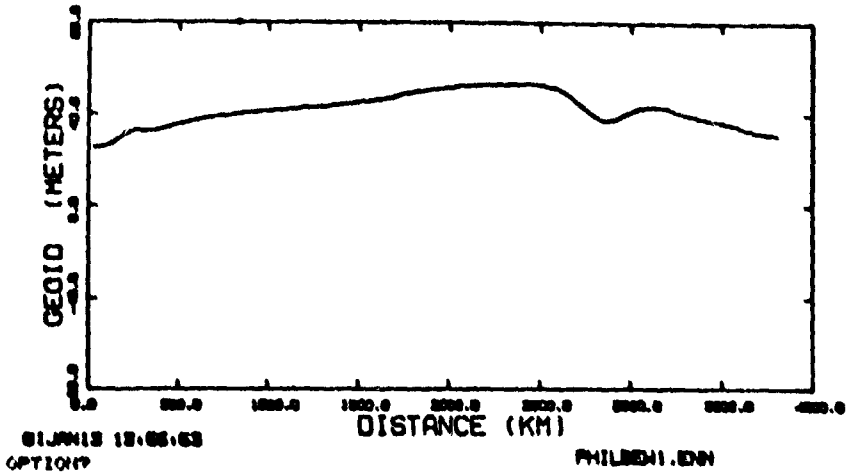
GEOID (METERS)
DISTANCE (KM)
PHILBDH1.EDN

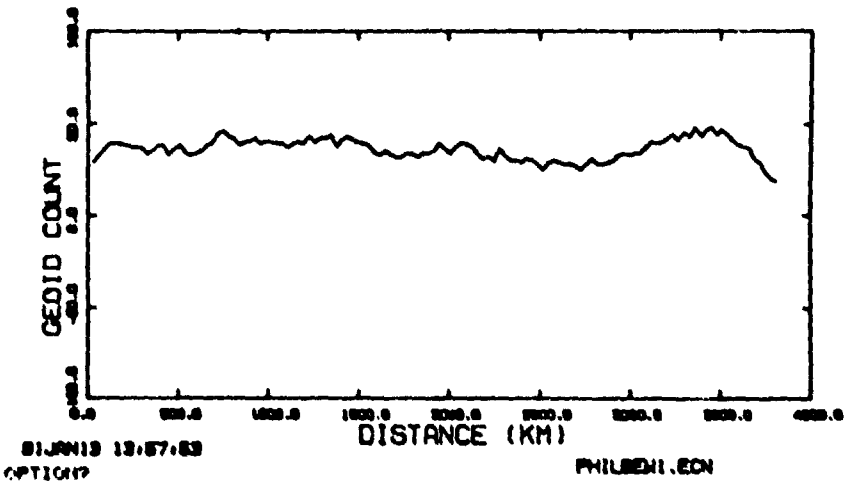
GEOID COUNT
DISTANCE (KM)
PHILBDH1.EDN

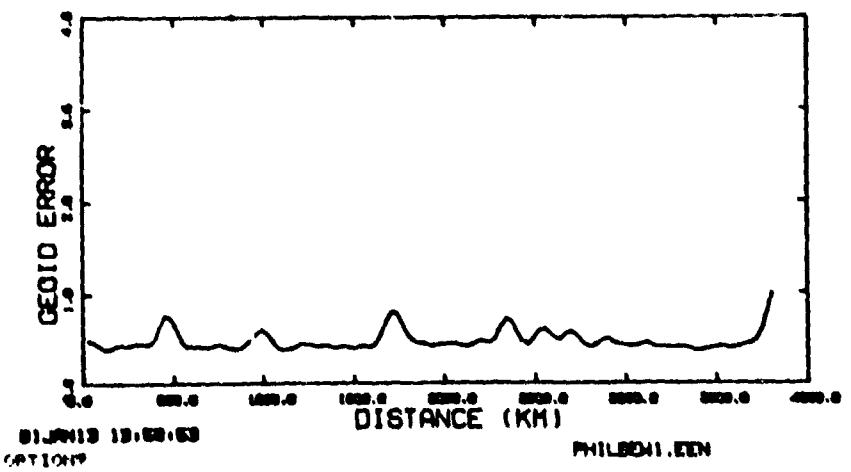
GEOID ERROR
DISTANCE (KM)
PHILBDH1.EEN

fig 8